MnO@1-D carbon composites from the precursor $C_4H_4MnO_6$ and their high-performance in lithium batteries†

Xiaona Li,[a] Yongchun Zhu,*[a] Xing Zhang,[a] Jianwen Liang[a] and Yitai Qian*[ab]

MnO@1-D carbon composites were synthesized simultaneously through a single heating procedure using $C_4H_4MnO_6$ as the precursor for both the MnO and 1-D carbon. MnO nanoparticles are uniformly dispersed inside or adhered to the surface of the 1-D carbon nanotubes, and these carbon nanotubes overlap each other to form carbon scaffolds. As an anode for lithium-ion batteries, the MnO@1-D carbon composites deliver a reversible capacity of 1482 mA h g^{-1} at a current density of 200 mA g^{-1}. When the current density rises to 1460 mA g^{-1}, the capacity remains at 810 mA h g^{-1} even after 1000 cycles. Such a unique carbon structure can act as a scaffold for MnO, which not only improves the electronic conductivity, but also provides a support for loading MnO nanoparticles. This synchronous process may pave a way to obtain such uniform and stable electrode materials with enhanced performance, which may find use in other applications such as catalysis, water treatment and supercapacitors.

1. Introduction

Transition metal oxides (TMOs) have attracted wide attention as anode materials due to their high theoretical capacities.[1–6] As one of many attractive anode materials for lithium-ion batteries, MnO has a high theoretical lithiation capacity (755.6 mA h g^{-1}), relatively low electrochemical motivation force (emf) (1.032 V *vs.* Li/Li$^+$), low cost, good safety characteristics and natural abundance.[7,8] However, like many other TMOs, the practical application of MnO is frustrated by its extremely low electronic conductivity[7,9] and its poor cycling performance resulting from huge volume changes and aggregation during the charge–discharge process due to the generation of Li_2O.[10] Combining with various forms of carbon materials is considered to be effective for overcoming these shortcomings. The existence of carbon could not only enhance the conductivity, but could also serve as a buffer to cushion the stress during lithiation and delithiation.[11–15]

In recent years, various kinds of MnO–C composites have been synthesized using different methods and employed as anode materials in lithium-ion batteries. For example, porous MnO–C core–shell nanotubes were prepared by thermally annealing a mixture of Mn_3O_4 nanotubes and glucose in an argon atmosphere. The obtained MnO–C nanotubes delivered a reversible charge capacity of 763.3 mA h g^{-1} after 100 cycles at 100 mA g^{-1}.[11] MnO–C nanoparticles were synthesized based on a carbothermal reduction process of Mn_3O_4 nanoparticles, with a high reversible capacity of 939.3 mA h g^{-1} after 30 cycles at 75.5 mA g^{-1}.[14] Through electrospinning and subsequent carbonization treatment, MnO@carbon core–shell nanofibers were obtained. As an anode material for lithium-ion batteries, they delivered an initial discharge capacity of 665.6 mA h g^{-1}, and the discharge capacity of the 50th cycle retained 99.7% of that of the 2nd cycle.[16] In our previous work, MnO@C core–shell nanoplates with controllable shell thickness were prepared *via* thermal treatment deposition of acetylene from a precursor of $Mn(OH)_2$ nanoplates, which displayed a high reversible capacity of ~770 mA h g^{-1} at a current density of 200 mA g^{-1}.[15] Therefore, it has been demonstrated that MnO–C composites are a good way to improve the electrochemical properties of pure MnO.

One dimensional (1D) nanostructures have drawn great attention as anode materials for LIBs, since they not only provide a flexible buffer to accommodate the volume change during lithium insertion–extraction, but also possess direct one-dimensional electronic pathways for efficient charge transport, thus increasing the conductivity of the electrode. In this regard, several preparation methods have been employed to synthesize 1-D structured anode materials.[17–20]

In this paper, MnO@1-D carbon composites with MnO nanoparticles encapsulated or adhered to the surface of the 1-D carbon scaffold are obtained by annealing the 1-D $C_4H_4MnO_6$ precursor nanocomposites in an argon atmo-

[a]*Hefei National Laboratory for Physical Science at Microscale and Department of Chemistry, University of Science and Technology of China, Hefei, 230026, P.R. China. E-mail: ychzhu@ustc.edu.cn; Tel: +86-551-63601589*

[b]*School of Chemistry and Chemical Engineering, Shandong University, Jinan, 250100, P.R. China. E-mail: ytqian@ustc.edu.cn; Tel: +86-551-63607234*

† Electronic supplementary information (ESI) available. See DOI: 10.1039/c3ra41132j

sphere. As an anode for lithium-ion batteries, MnO@1-D carbon composites exhibited a higher lithium storage capacity of 1482 mA h g^{-1} at a current density of 200 mA g^{-1}. When the current density rises to 1460 mA g^{-1}, the capacity still remains at 810 mA h g^{-1} even after 1000 cycles.

2. Experimental

2.1. Preparation of the 1-D C$_4$H$_4$MnO$_6$ precursor

In a typical synthesis of 1-D C$_4$H$_4$MnO$_6$ nanorods, 0.2212 g of MnCl$_2$·4H$_2$O and 0.168 g tartaric acid were first dissolved in 30 mL deionized water at room temperature under magnetic stirring. Then 10 mL of 0.25 M NaOH was added dropwise to the above solution. The mixture was stirred for 0.5 h and then was poured into and sealed in a 60 mL Teflon-lined stainless steel autoclave. The autoclave was heated to and maintained at 150 °C for 6 h and then cooled to room temperature naturally. The white product was collected by filtration, washed with distilled water and ethanol, and then dried under vacuum at 60 °C for 6 h.

2.2. Preparation of the MnO@1-D carbon composites

The as-prepared 1-D C$_4$H$_4$MnO$_6$ was heated in a high purity argon atmosphere at 500 °C for 4 h, followed by natural cooling to room temperature. The ramping rate was 2 °C min^{-1}.

2.3. Characterization

The X-ray powder diffraction (XRD) patterns were obtained on a Philips X'pert PRO SUPER diffractometer equipped with graphite monochromatized Cu Kα radiation (λ = 1.541874 Å). The scanning electron microscopy (SEM) images were taken with a JEOL-JSM-6700F field emission scanning electron microscope. The transmission electron microscopy (TEM) images were recorded on a Hitachi Model H-7650 transmission electron microscope, using an electron kinetic energy of 100 kV. The high-resolution transmission electron microscopy (HRTEM) images and selected area electron diffraction (SAED) patterns were taken on a JEOL 2010 high-resolution transmission electron microscope performed at an acceleration voltage of 200 kV. The Brunauer–Emmett–Teller (BET) surface area of the products was determined by using a Tristar II 3020M apparatus. Thermogravimetric analysis (TGA) was performed with a TGA-2050 (TA Corp.) under N$_2$ flow. The chemical composition and the valence states of constituent elements were analyzed by X-ray photoelectron spectroscopy (XPS; monochromatic Al Kα X-ray source, Kratos Analytical Ltd.). A Vario ELIII was used to measure the carbon content. Raman spectra were recorded at ambient temperature with a NEXUS 670 FT-IR Raman spectrometer.

Electrochemical measurements were carried out using coin-type 2016 cells. For working electrodes, the MnO@1-D carbon composites were mixed with acetylene black, and a polyvinylidene fluoride (PVDF) binder in a weight ratio of 60 : 30 : 10. Lithium metal was used as the counter electrode, and the separator was a Celgard 2400 microporous membrane. The electrolyte was 1 mol L^{-1} LiPF$_6$ solution in ethylene carbonate
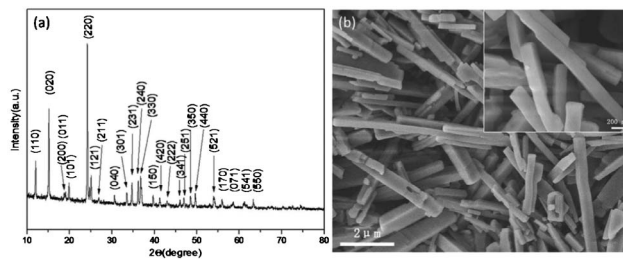

Fig. 1 (a) XRD pattern and (b) SEM images of the 1-D C$_4$H$_4$MnO$_6$ nanorods.

and dimethyl carbonate solution (EC + DMC) (1 : 1) in volume. The battery cells were assembled in an argon-filled glovebox and the charge–discharge tests were performed on a Land automatic battery tester (Wuhan, China) for a voltage window of 0.01–3.0 V($vs.$ Li/Li$^+$) at room temperature. Cyclic voltammetry (CV) was performed on a CHI 660C electrochemical workstation (Shanghai) using a coin cell at a scan rate of 0.1 mV s^{-1} from 0.001 V to 3.0 V.

3. Results and discussion

Fig. 1a is the XRD pattern of the precursor prepared by a hydrothermal process at 150 °C for 6 h. All the diffraction peaks can be indexed to orthorhombic C$_4$H$_4$MnO$_6$ (a = 9.437 Å, b = 11.693 Å, c = 5.068 Å, JCPDF No. 33-0910, space group: $Pnnm$). The morphology of the 1-D C$_4$H$_4$MnO$_6$ nanorods was analyzed by scanning electron microscopy (SEM) in Fig. 1b. Most of them were 1-D nanorods with a diameter of 200 nm and a length of up to several micrometers.

The TGA technique was used to analyze the thermal behavior of the C$_4$H$_4$MnO$_6$ samples and thus could provide the necessary data for the following decomposition process. As shown in the TGA curve of the 1-D C$_4$H$_4$MnO$_6$ nanorods under a N$_2$ atmosphere (Fig. 2), there is a huge weight loss process (56.66%) from 200 to 500 °C, which can be ascribed to the decomposition of C$_4$H$_4$MnO$_6$ to the final MnO, the 1-D carbon and carbon oxides. We chose 500 °C as the annealing
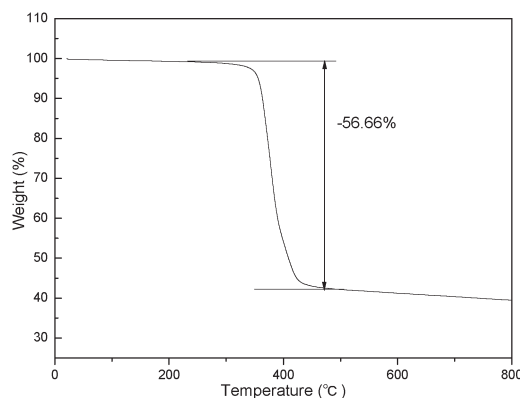

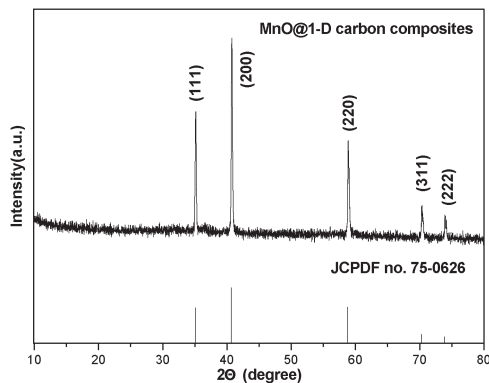**Fig. 2** TGA curve of the C$_4$H$_4$MnO$_6$ nanorods under N$_2$.

Fig. 3 XRD pattern of the MnO@1-D carbon composites.

Fig. 5 XPS spectra of MnO@1-D carbon composites: (a) survey spectrum, (b) Mn 2p, (c) O 1s and (d) C 1s.

temperature since the weight of the product remains almost unchanged above 500 °C from the TGA curve.

Fig. 3 shows the typical XRD pattern of the products after $C_4H_4MnO_6$ is heated in a high purity argon atmosphere at 500 °C for 4 h. All of the sharp diffraction peaks can be assigned to the cubic phase of MnO (JCPDS Card No. 75-0626, space group: $Fm\bar{3}m$). No peaks from other phases were detected.

The products were further analyzed by Raman spectroscopy (Fig. 4). According to a previous report,[21] MnO is easily transformed into Mn_3O_4, caused by beam irradiation when the beam intensity is more than 1.1 mW, during the Raman measurement. Therefore, the vibrational band at 644 cm^{-1} and bands below 400 cm^{-1} belong to Mn_3O_4 rather than MnO. There are two peaks at 1358 and 1601 cm^{-1}, which are attributed to the typical disordered band (D band) and the graphene band (G band) of carbon. The ratio between the D and G band is found to correlate to the nature of carbon. The ID/IG value (ratio of the intensity of D Raman peak and G Raman peak) of the MnO@1-D carbon composites is 0.75, which is much higher than fully graphitized carbon,[22] revealing a relatively amorphous state of the carbon in the MnO@1-D carbon composites.
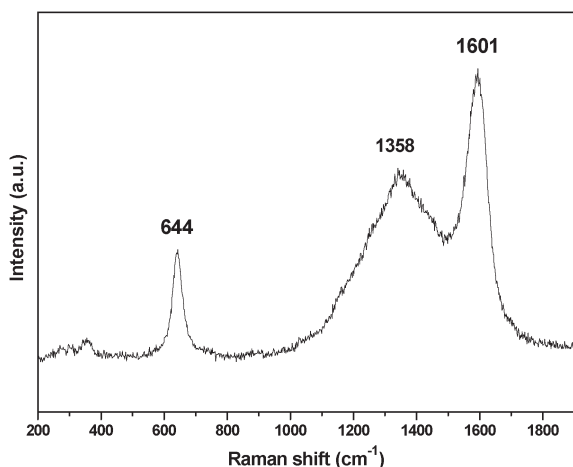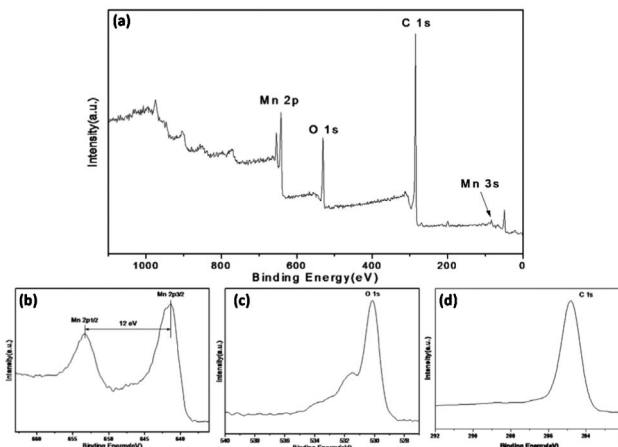
The XPS survey spectrum for the as-obtained sample is presented in Fig. 5. The main peaks observed in the XPS survey spectrum were C 1s (284.8 eV), O 1s (530.15 eV) and Mn 2p. The values of the binding energies obtained for $Mn2p_{3/2}$ and $Mn2p_{1/2}$ were located at 641.35 and 653.35 eV, respectively, which are in good agreement with those reported for MnO.[23,24,28] In addition, the obtained spin–energy separation is 12.0 eV, which further confirms the presence of MnO. The at% of Mn : C is 8.33 : 76.77, calculated based on the XPS spectrum.

The morphology and microstructure of the MnO@1-D carbon composites are clarified by the FESEM and TEM images in Fig. 6. The typical overall FESEM image (Fig. 6a) shows that the obtained products are 1-D nanorods with a length of several micrometers attached by small nanoparticles. Detailed microstructural analysis of these nanostructures was performed by TEM. Fig. 6b is a high magnification TEM image of the products, which shows that the dark nanoparticles are either encapsulated inside the pale 1-D scaffold or adhered to the surface of the 1-D scaffold. The HRTEM image of the composites is shown in Fig. 6c. The measured spacing of the lattice planes for the encapsulated nanoparticles is 0.256 nm, which is consistent with the {111} planes of cubic MnO. The randomly marked area shown by the circles in Fig. 6c indicates that the 1-D scaffold is amorphous. The SAED pattern inset in Fig. 6c is indexed to the {220} crystal planes of MnO. The HRTEM image and ED pattern further confirm that the structure is composed of MnO nanoparticles encapsulated inside or adhered to the surface of the 1-D carbon scaffold. After the removal of the MnO nanoparticles, only the 1-D porous carbon scaffolds, which were composed of interconnected amorphous carbon were left (Fig. 7). The 1-D porous carbon scaffolds linked to each other to form the whole electrically conducting carbon network. Analyzed on a Vario ELIII, the carbon content of the MnO@1-D carbon composites is about 10.63%. This value is much lower than the carbon content on the surface of the final samples according to the

**Fig. 4** Raman spectrum of the MnO@1-D carbon composites.
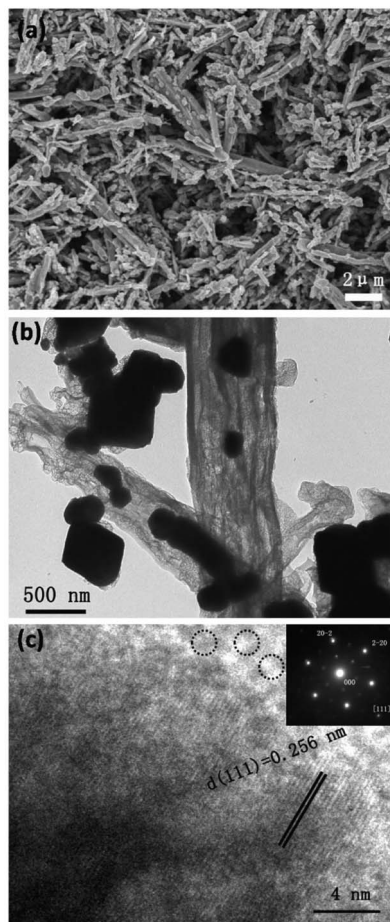
Fig. 6 (a) FESEM image, (b) TEM image, (c) HRTEM image and SAED pattern (inset) of the MnO@1-D carbon composites.

XPS survey spectrum, which suggests that the MnO is partially located inside the final amorphous carbon.

The lithium-storage properties of the as-prepared MnO@1-D carbon composites were characterized by galvanostatic discharge–charge measurements. All tested specific capacities were calculated on the mass of the whole composites (MnO + C). Fig. 8a shows the cyclic voltammetry (CV) curves of the MnO@1-D carbon composites for the first five cycles in the voltage range 0.001–3.0 V *versus* Li/Li$^+$ at a scan rate of 0.1 mV s^{-1}. In the first cycle, two peaks around 0.1 and 0.45 V can be seen in the first cathodic process, which can be assigned to the
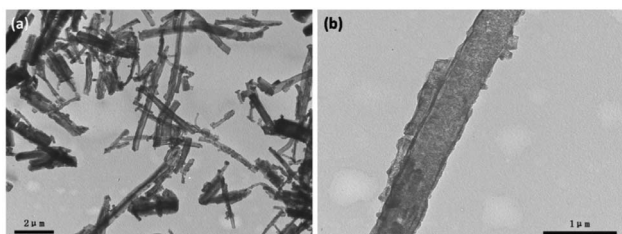
Fig. 7 TEM images of the 1-D porous carbon scaffolds.
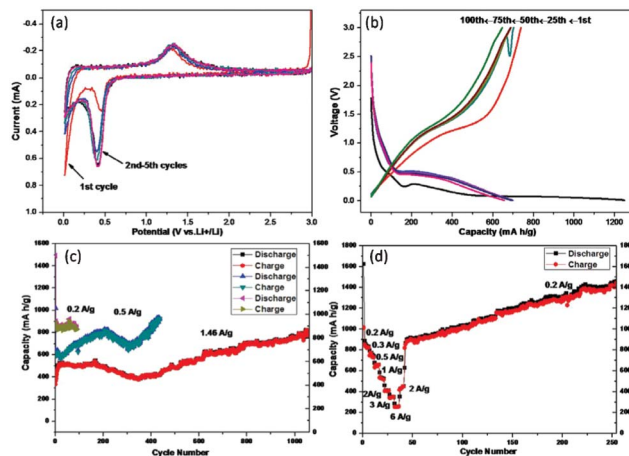
Fig. 8 (a) CV curves for the MnO@1-D carbon composites measured at a scan rate of 0.1 mV s^{-1} between 0.001 and 3.0 V. (b) Galvanostatic discharge–charge profiles of the MnO@1-D carbon composites at a current rate of 0.5 A g^{-1}. (c) Cycling performance of the MnO@1-D carbon composites at three current densities of 0.2, 0.5 and 1.460 A g^{-1}. (d) Rate capability tests at various current densities for the MnO@1-D carbon composites.

reduction of MnO to metallic Mn, the formation of amorphous Li$_2$O and the formation of a SEI layer with a reversible polymer/gel like film.[25] During the anodic process, there is only one peak at 1.25 V which is ascribed to the regeneration of MnO and decomposition of Li$_2$O.[26] The CV curves for the subsequent four cycles are substantially different from the first cycle. It can be observed that the reduction peak shifts to 0.39 V, which is due to Mn^{2+} to Mn conversion, while the oxidation peak is located at 1.25 V, which corresponds to the metallic Mn to Mn^{2+} conversion. From the second cycle onward, the reduction peaks in the cathodic scan and the oxidation peaks in the anodic scan overlap very well, indicating that the electrode of the MnO@1-D carbon composites exhibits good stability and cyclability for the insertion and extraction of lithium ions.[27]

Fig. 8b shows the 1st, 25th, 50th, 75th and 100th charge and discharge profiles of the MnO@1-D carbon composites at a constant current density of 0.5 A g^{-1}. The plateau around 0.25 V in the first discharge curve was attributed to the reduction of MnO to Mn. For the initial charge curve, the electrode shows a slope in the voltage range between 1.0 and 1.5 V, related to the oxidation of Mn to MnO. In the following cycling process, the discharge plateau shifted to ~0.5 V, this phenomenon is consistent with other transition metal oxides.[29] The initial discharge and charge capacities of the MnO@1-D carbon composites are 1249 and 738 mA h g^{-1}, respectively. The low coulombic efficiency (59%) of the MnO@1-D carbon composites in the first cycle is attributed to the pulverization of the active materials and the formation of a solid electrolyte interphase (SEI) layer according to previous reports.[7,30] From the second cycle onwards, the discharge curve stabilizes at ~660 mA h g^{-1}, which indicates the excellent stability of the MnO@1-D carbon composite electrodes.

The cycling performance of the MnO@1-D carbon composites was further investigated (Fig. 8c). At low current densities of 0.2 A g^{-1}, the discharge capacities of the sample remained stable, cycling at about 860 mA h g^{-1} for the next tested cycles. It is interesting to note that the specific capacity gradually increased at the higher current density of 0.5 A g^{-1}, which is also reported in other MnO$_x$-based[7,11,28,31] and transition metal oxides.[32,33] It is probably attributed to increased electrochemical access to the active material as cycling proceeds and the reversible growth of a polymeric gel-like film resulting from kinetically activated electrolyte degradation. Not all of the surface is covered by the polymer layer during the first discharge, since the internal surface of the active materials within the pores is more difficult to access. Thus, the polymeric surface layer builds up slowly. We can see that even at the high current density of 1.46 A g^{-1}, the electrode can deliver a capacity as high as ∼520 mA h g^{-1} after 200 cycles. After 350 cycles, the capacity can gradually increase back to ∼810 mA h g^{-1} by the 1000th cycle.

To better understand the electrochemical behavior of the MnO@1-D carbon composites, we also investigated their rate performance with respect to Li$^+$ insertion–extraction (Fig. 8d). The electrode was first cycled at 0.1 A g^{-1}, and then the rate performance was tested at current densities of 0.2, 0.3, 0.5, 1, 2, 3, and 6 A g^{-1}; where the average discharge capacities of 850, 760, 660, 530, 420, 350 and 250 mA h g^{-1}, respectively, were obtained after five charge and discharge cycles at each of these current densities. In addition, the capacities are relatively stable at these current densities. Upon altering the current density stepwise back to 0.2 A g^{-1}, a discharge capacity as high as 1482 mA h g^{-1} could be recovered gradually. This demonstrates that the MnO@1-D carbon composites have great potential as a high-rate anode material in lithium-ion batteries.

Therefore, we could probably attribute the prominent performance of the MnO@1-D carbon composites obtained at 500 °C for 4 h to the following aspects. First, the 1-D carbon structure could ensure efficient electron transport along the longitudinal direction, and this is crucial to the rate performance of the electrode material. Second, the MnO@1-D carbon composites have better mechanical toughness than pure metal oxides, which will benefit the long-term cyclic stability. Though the collapse and reconstruction of the active MnO particles are inevitable during the cycling process, the reconstructed MnO particles can still be loaded into the whole carbon scaffold, which can connect electrochemically with the amorphous carbon scaffold closely and facilitate charge–discharge transfer.[34,35] This can be confirmed by the SEM and TEM images of the electrodes after cycling (shown in Fig. 9), which indicate that not only are the MnO nanoparticles still maintained in the whole carbon scaffold, but also the structure of the carbon scaffold is not damaged. The carbon scaffold with such a unique structure not only improves the electronic conductivity, but also may accommodate the volume expansion–contraction during the Li$^+$ insertion–extraction processes because of its good mechanical stability and strain accommodation.[36,37] Furthermore, the special structure of the 1-D carbon prepared from the *in situ* approach can act as a scaffold for MnO, which can provide a support for loading the MnO nanoparticles and facilitates the mass transport of the solvated ions in the electrolyte to the MnO surface. In this regard, both the specific capacity and cycling performance of the MnO@1-D carbon composites can be improved effectively.

4. Conclusions

In conclusion, we have designed an *in situ* synthesis route to MnO@1-D carbon composites annealed from a 1-D C$_4$H$_4$MnO$_6$ precursor. The MnO@1-D carbon composites exhibit high performance at high constant current density for lithium-ion batteries, providing reversible capacities of 1482 mA h g^{-1} at a current density of 200 mA g^{-1} after the rate performance test and 810 mA h g^{-1} at 1460 mA g^{-1}. The final MnO nanoparticles and the whole stable carbon skeleton are obtained synchronously. The high capability and good cycling performance may be attributed to such a unique carbon skeleton, which favors fast electron transportation and high structural stability during the reversible charge–discharge process.

Acknowledgements

Fig. 9 SEM and TEM images of the electrodes after 400 cycles, at a current rate of 0.5 A g^{-1}.

Notes and references

1 Y. M. Sun, X. L. Hu, W. Luo and Y. H. Huang, *J. Mater. Chem.*, 2012, **22**, 13826.

2 Y. G. Li, B. Tan and Y. Y. Wu, *Nano Lett.*, 2008, **8**, 265.

3 X. J. Zhu, Y. W. Zhu, S. Murali, M. D. Stoller and R. S. Ruoff, *ACS Nano*, 2011, **5**, 3333.

4 E. Kang, Y. S. Jung, A. S. Cavanagh, G. H. Kim, S. M. George, A. C. Dillon, J. K. Kim and J. Lee, *Adv. Funct. Mater.*, 2011, **21**, 2430.
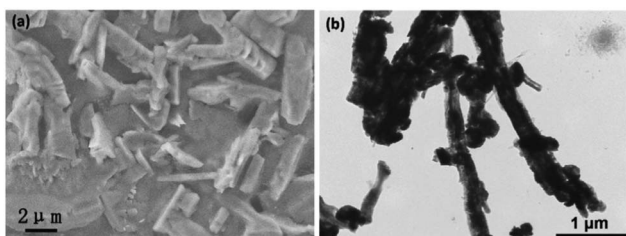
5 J. Gao, M. A. Lowe and H. D. Abruña, *Chem. Mater.*, 2011, **23**, 3223.

6 Y. M. Sun, X. L. Hu, W. Luo and Y. H. Huang, *ACS Nano*, 2011, **5**, 7100.

7 K. F. Zhong, X. Xia, B. Zhang, H. Li, Z. X. Wang and L. Q. Chen, *J. Power Sources*, 2010, **195**, 3300.

8 H. L. Wang, L. F. Cui, Y. Yang, H. S. Casalongue, J. T. Robinson, Y. Y. Liang, Y. Cui and H. J. Dai, *J. Am. Chem. Soc.*, 2010, **132**, 13979.

9 Y. J. Mai, D. Zhang, Y. Q. Qiao, C. D. Gu, X. L. Wang and J. P. Tu, *J. Power Sources*, 2012, **216**, 201.

10 F. Cheng, Z. Tao and J. Liang, *Chem. Mater.*, 2008, **20**, 667.

11 G. L. Xu, Y. F. Xu, H. Sun, F. Fu, J. T. Li, S. H. Yang and S. G. Sun, *Chem. Commun.*, 2012, **48**, 8502.

12 C. Chae, J. H. Kim, J. M. Kim, Y. K. Sunc and J. K. Lee, *J. Mater. Chem.*, 2012, **22**, 17870.

13 Y. M. Liu, X. Y. Zhao, F. Li and D. G. Xia, *Electrochim. Acta*, 2011, **56**, 6448.

14 S. R. Li, Y. Sun, S. Y. Ge, Y. Qiao, Y. M. Chen, I. Lieberwirth, Y. Yu and C. H. Chen, *Chem. Eng. J.*, 2012, **192**, 226.

15 X. Zhang, Z. Xing, L. L. Wang, Y. C. Zhu, Q. W. Li, Y. T. Qian and X. Y. Shen, *J. Mater. Chem.*, 2012, **22**, 17864.

16 G. Yang, Y. H. Li, H. M. Ji, H. Y. Wang, P. Gao, L. Wang and X. F. Jiang, *J. Power Sources*, 2012, **216**, 353.

17 Y. L. Ding, C. Y. Wu, H. M. Yu, J. Xie, G. S. Cao, T. J. Zhu, X. B. Zhao and Y. W. Zeng, *Electrochim. Acta*, 2011, **56**, 5844.

18 W. Luo, X. L. Hu, Y. M. Sun and Y. H. Huang, *Phys. Chem. Chem. Phys.*, 2011, **13**, 16735.

19 W. Luo, X. Hu, Y. Sun and Y. Huang, *ACS Appl. Mater. Interfaces*, 2013, **5**, 1997.

20 J. C. Guo, Q. Liu, C. S Wang and M. R. Zachariah, *Adv. Funct. Mater.*, 2012, **22**, 803.

21 I. Rusakova, T. Ould-Ely, C. Hofmann, D. Prieto-Centurión, C. S. Levin, N. J. Halas, A. Lüttge and K. H. Whitmire, *Chem. Mater.*, 2007, **19**, 1369.

22 Y. He, L. Huang, X. Li, Y. Xiao, G. L. Xu, J. T. Li and S. G. Sun, *J. Mater. Chem.*, 2011, **21**, 18517.

23 D. P. Dubal, D. S. Dhawale, R. R. Salunkhe and C. D. Lokhande, *J. Electroanal. Chem.*, 2010, **647**, 60.

24 C.-T. Hsieh, C. Y. Lin and J. Yi. Lin, *Electrochim. Acta*, 2011, **56**, 8861.

25 M. S. Wu, P. C. J. Chiang, J. T. Lee and J. C. Lin, *J. Phys. Chem. B*, 2005, **109**, 23279.

26 X. W. Li, D. Li, L. Qiao, X. H. Wang, X. L. Sun, P. Wang and D. Y. He, *J. Mater. Chem.*, 2012, **22**, 9189.

27 B. Sun, Z. Chen, H.-S. Kim, H. Ahn and G. Wang, *J. Power Sources*, 2011, **196**, 3346.

28 O. Delmer, P. Balaya and L. Kienle, *Adv. Mater.*, 2008, **20**, 501.

29 Y. H. Yu, Q. Yang, D. H. Teng, X. P. Yang and S. Ryu, *Electrochem. Commun.*, 2010, **12**, 1187.

30 J. Z. Wang, N. Du, H. Wu, H. Zhang, J. X. Yu and D. R. Yang, *J. Power Sources*, 2013, **222**, 32.

31 Y. M. Sun, X. L. Hu, W. Luo, F. F. Xia and Y. H. Huang, *Adv. Funct. Mater.*, 2012, DOI: 10.1002/adfm.201202623.

32 X. H. Rui, H. t. Tan, D. h. Sim, H. H. Hng, R. Yazami, T. M. Lim and Q. Y. Yan, *J. Power Sources*, 2013, **222**, 97.

33 J. J. Zhang, Y. F. Sun, Y. Yao, T. Huang and A. s. Yu, *J. Power Sources*, 2013, **222**, 59.

34 H. Y. Wang, P. Gao, S. F. Lu, H. D. Liu, G. Yang, J. Pinto and X. F. Jiang, *Electrochim. Acta*, 2011, **58**, 44.

35 Y. Yu, L. Gu, C. Wang, A. Dhanabalan and P. A. Aken, *Angew. Chem., Int. Ed.*, 2009, **48**, 6485.

36 Y. G. Li, B. Tan and Y. Y. Wu, *Nano Lett.*, 2008, **8**, 265.

37 S. W. Kim, H. W. Lee, P. Muralidharan, D. H. Seo, W. S. Yoon, D. K. Kim and K. Kang, *Nano Res.*, 2011, **4**, 505.

This journal is © The Royal Society of Chemistry 2013